Supplementary material for LHCb-PAPER-2019-006

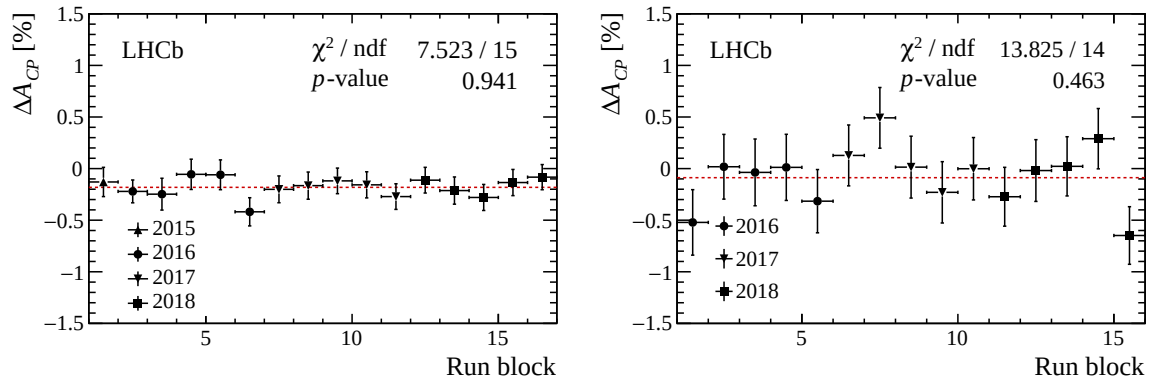

Figure 2: Measurements of ΔA_{CP} in time-ordered data-taking subsamples (referred to as run blocks) for (left) prompt and (right) semileptonic samples. The uncertainties are statistical only. The horizontal red-dashed lines show the central values of the nominal results.

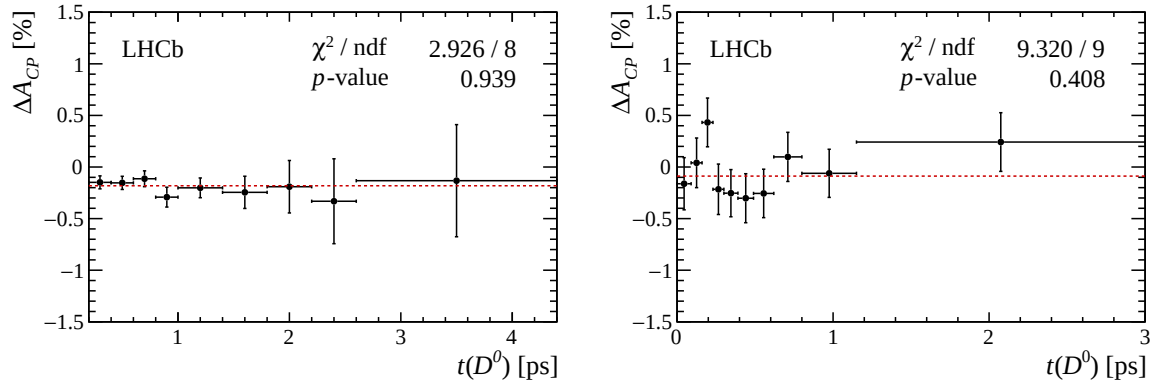

Figure 3: Measurements of ΔA_{CP} in bins of D^0 decay time for (left) prompt and (right) semileptonic samples. In each plot, the last bin on the right also includes a few overflow candidates. The uncertainties are statistical only. The horizontal red-dashed lines show the central values of the nominal results.

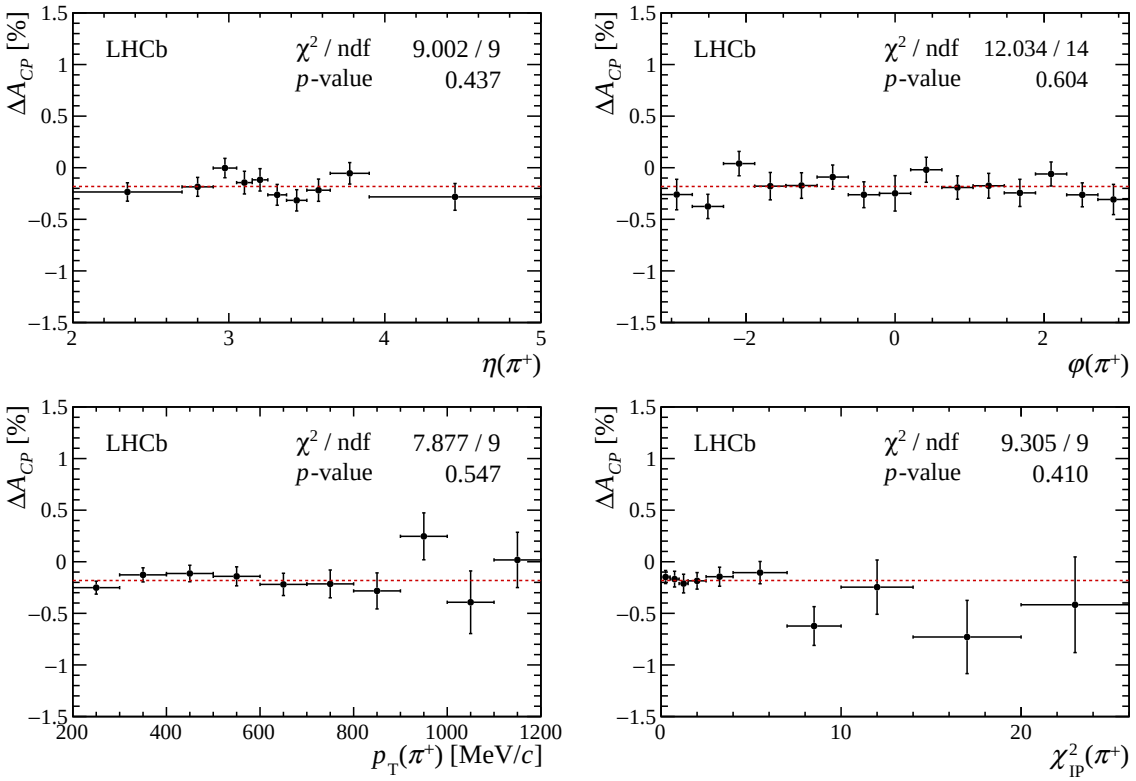

Figure 4: Measurements of ΔA_{CP} in bins of (top left) pseudorapidity, (top right) azimuthal angle, (bottom left) transverse momentum and (bottom right) $\chi^2_{\rm IP}$ of tagging pions for the prompt sample. In each plot but that of the azimuthal angle, the last bin on the right also includes a few overflow candidates. The uncertainties are statistical only. The horizontal red-dashed lines show the central value of the nominal result.

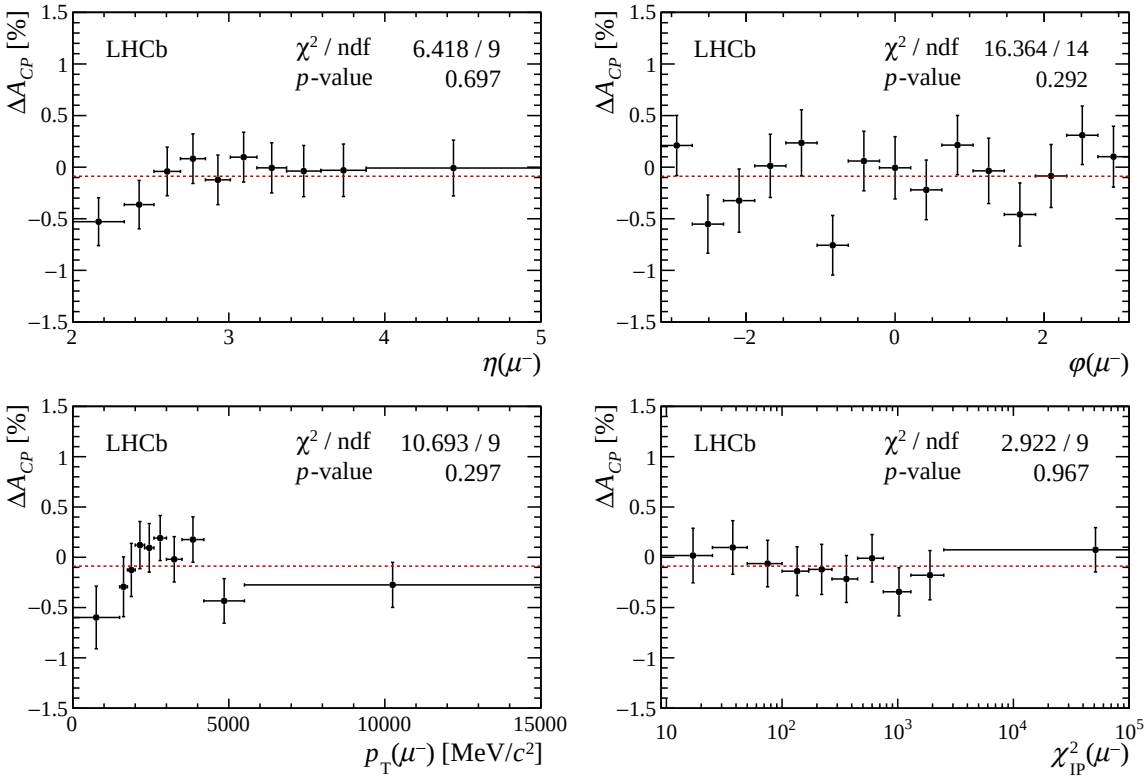

Figure 5: Measurements of ΔA_{CP} in bins of (top left) pseudorapidity, (top right) azimuthal angle, (bottom left) transverse momentum and (bottom right) $\chi^2_{\rm IP}$ of tagging muons for the semileptonic sample. In each plot but that of the azimuthal angle, the last bin on the right also includes a few overflow candidates. The uncertainties are statistical only. The horizontal red-dashed lines show the central value of the nominal result.

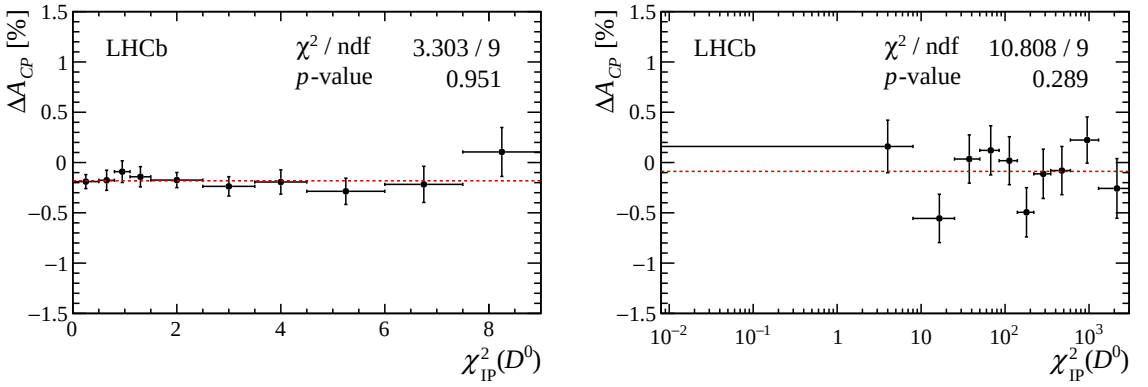

Figure 6: Measurements of ΔA_{CP} in bins of D^0 $\chi^2_{\rm IP}$ for (left) prompt and (right) semileptonic samples. In each plot, the last bin on the right also includes a few overflow candidates. The uncertainties are statistical only. The horizontal red-dashed lines show the central values of the nominal results.

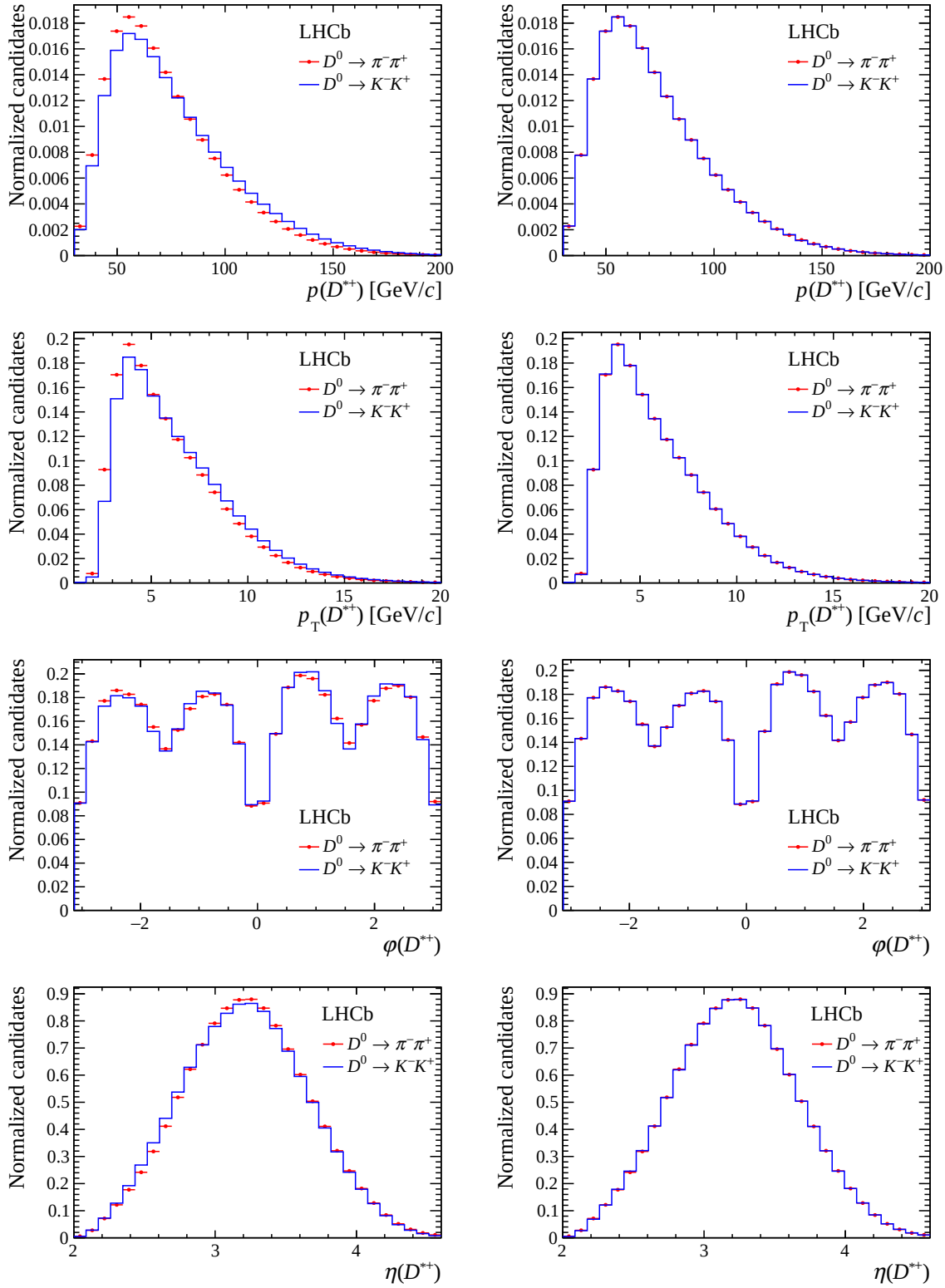

Figure 7: Background-subtracted distributions of momentum (p), transverse momentum ($p_{\rm T}$), azimuthal angle (φ) and pseudorapidity (η) of D^{*+} mesons for the prompt sample: (left column) before and (right column) after the weighting procedure for $D^0 \to K^-K^+$ and $D^0 \to \pi^-\pi^+$ decays, as indicated in the legends. The distributions are normalized to unit area.

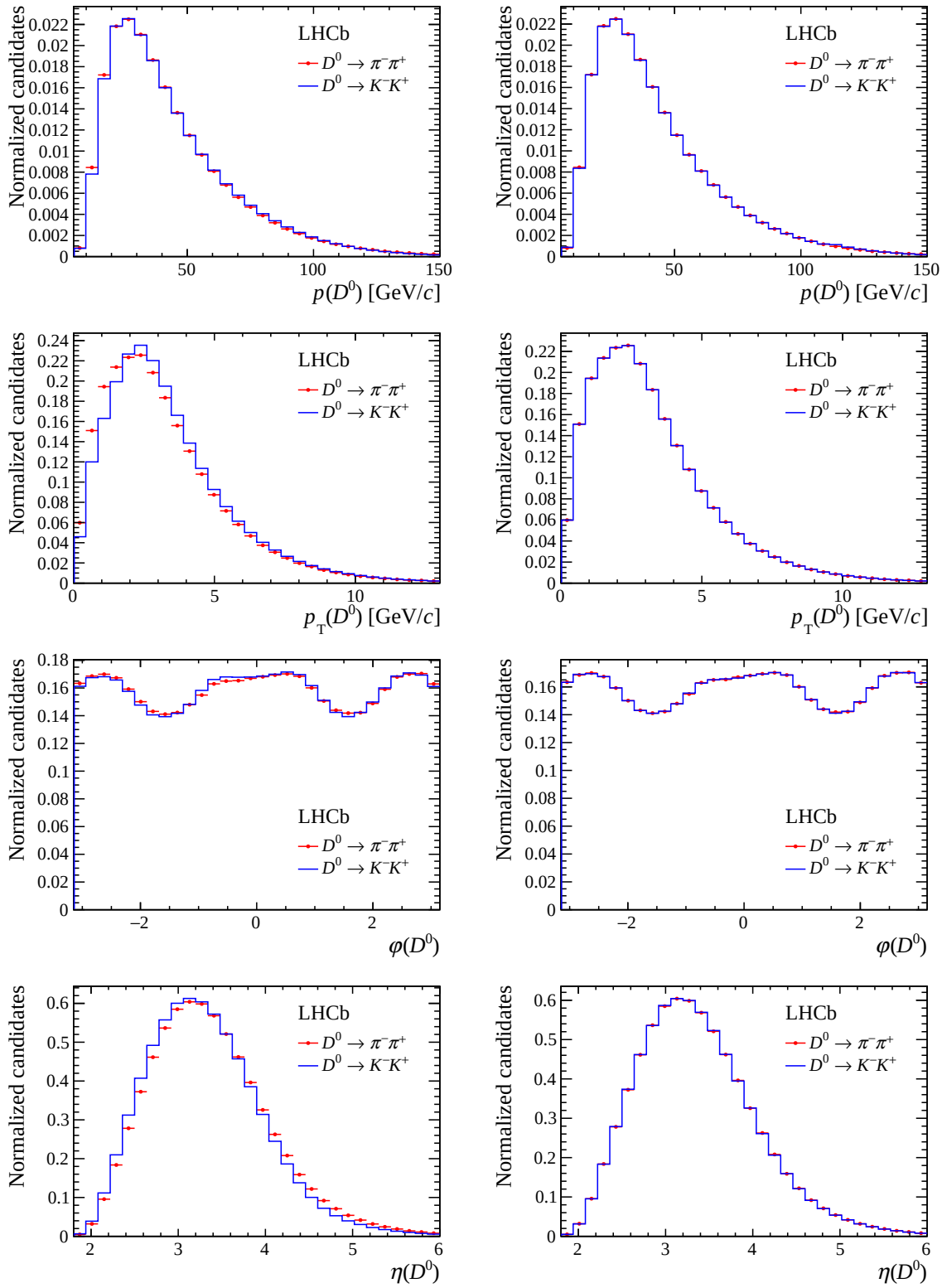

Figure 8: Background-subtracted distributions of momentum (p), transverse momentum ($p_{\rm T}$), azimuthal angle (φ) and pseudorapidity (η) of D^0 mesons for the semileptonic sample: (left column) before and (right column) after the weighting procedure for $D^0 \to K^-K^+$ and $D^0 \to \pi^-\pi^+$ decays, as indicated in the legends. The distributions are normalized to unit area.

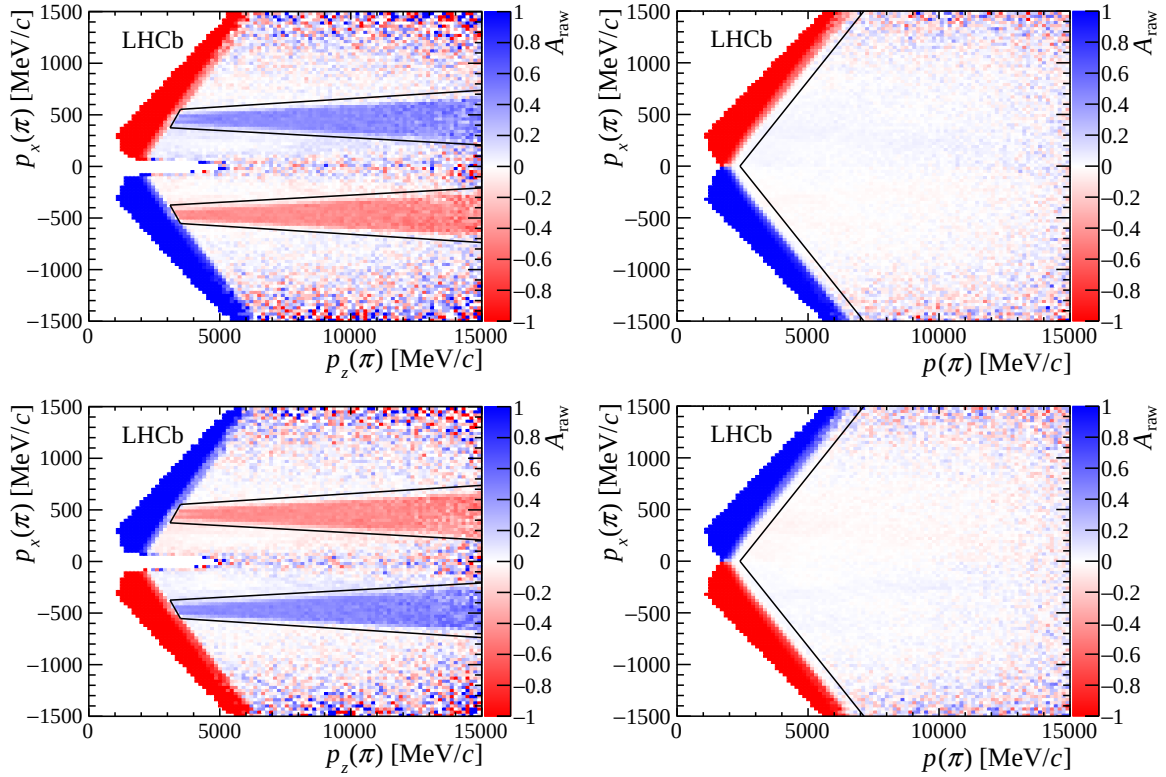

Figure 9: Raw asymmetries of the tagging pion for the π-tagged $D^0 \to K^-K^+$ sample, with the polarity of the magnet (top) up and (bottom) down. The plots on the left include only candidates with $|p_y/p_z| < 0.02$, *i.e.*, close to the horizontal plane, and the fiducial requirements used to exclude the kinematic region surrounding the beam pipe, characterized by large values of the raw asymmetry, are indicated as black lines (in addition to the forementioned requirement $|p_y/p_z| < 0.02$). The plots on the right include all candidates except those excluded by the beam-pipe fiducial requirements, and the black lines indicate the fiducial requirements used to exclude regions at the boundary of the detector acceptance, which are also characterized by large values of the raw asymmetry. Distributions for the $D^0 \to \pi^-\pi^+$ sample are very similar.

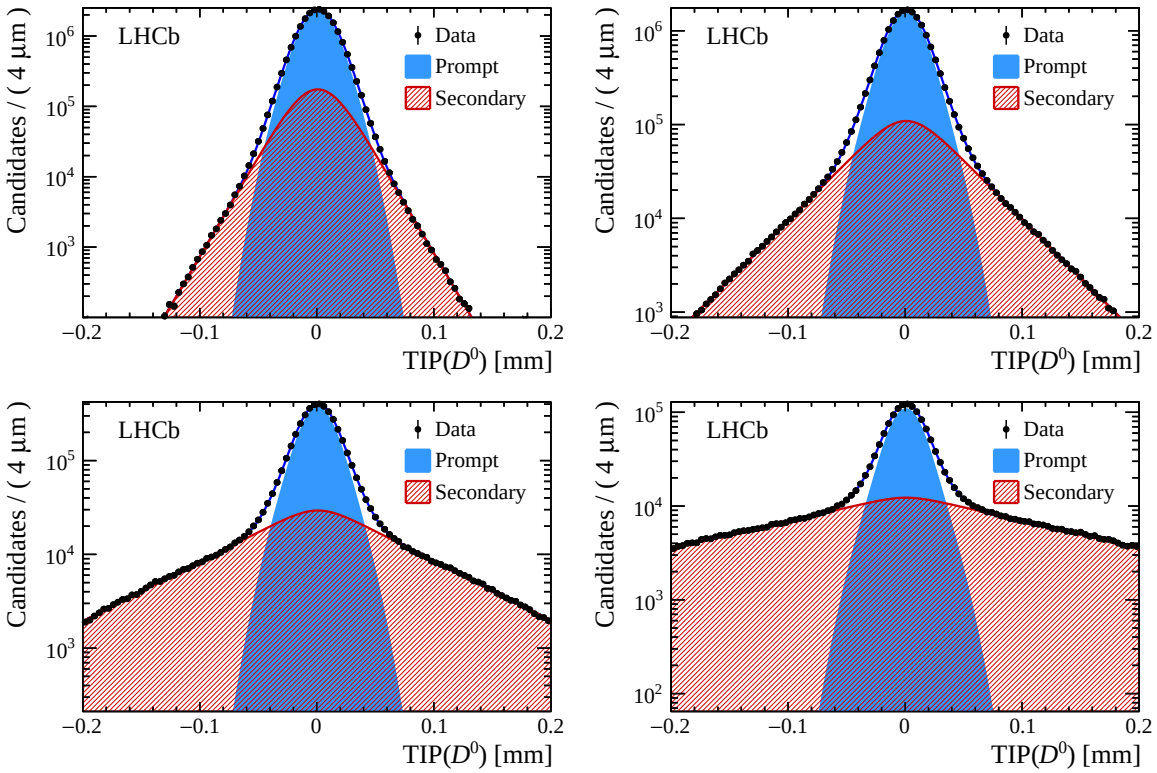

Figure 10: Distributions of the signed D^0 impact parameter in the plane transverse to the beam direction, TIP, in bins of reconstructed D^0 decay time, for the π-tagged $D^0 \to K^-K^+$ sample: (top left) $\tilde{t} < 1.5$, (top right) $1.5 < \tilde{t} < 3.0$, (bottom left) $3.0 < \tilde{t} < 4.5$ and (bottom right) $\tilde{t} > 4.5$, where $\tilde{t} \equiv t/\tau(D^0)$. The fit results are overlaid and the contributions from prompt and secondary decays are shown, as indicated in the legends. Distributions for the $D^0 \to \pi^-\pi^+$ sample are very similar.

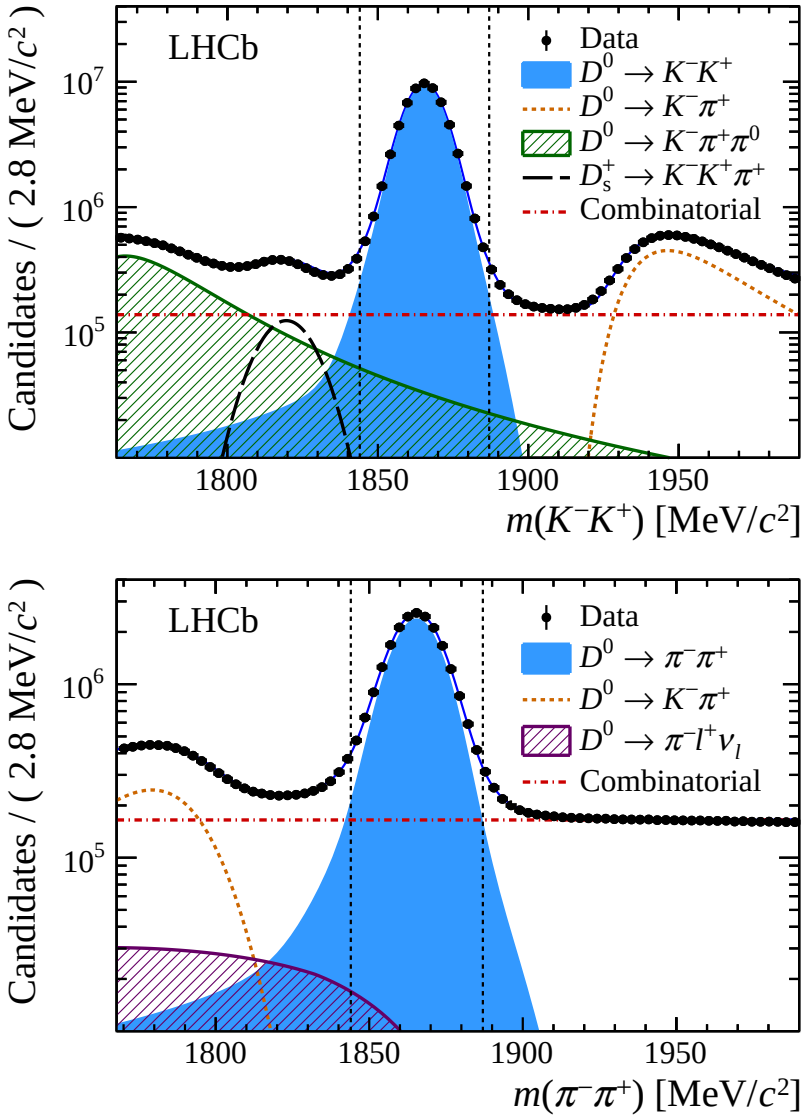

Figure 11: Invariant-mass distributions of (top) $D^0 \to K^-K^+$ and (bottom) $D^0 \to \pi^-\pi^+$ candidates in the prompt sample with fit results overlaid. These fits are used to determine the yields and raw asymmetries of (top) $D^0 \to K^-\pi^+\pi^0$ and (bottom) $D^0 \to \pi^- l^+ \nu_l$ backgrounds, whose mass shapes extend to the D^0-signal mass region. The various components included in the fit model are indicated in the legends.